Nebulin-deficient mice exhibit shorter thin filament lengths and reduced contractile function in skeletal muscle

Marie-Louise Bang,[1] Xiaodong Li,[1] Ryan Littlefield,[5] Shannon Bremner,[3,4] Andrea Thor,[2] Kirk U. Knowlton,[1] Richard L. Lieber,[3,4] and Ju Chen[1]

[1]Department of Medicine, [2]National Center for Microscopy and Imaging Research, [3]Department of Orthopaedic Surgery, and [4]Department of Bioengineering, Veterans Affairs Medical Center, University of California, San Diego, La Jolla, CA 92093
[5]Center for Cell Dynamics, Friday Harbor Laboratories, University of Washington, Friday Harbor, WA 98250

Nebulin is a giant modular sarcomeric protein that has been proposed to play critical roles in myofibrillogenesis, thin filament length regulation, and muscle contraction. To investigate the functional role of nebulin in vivo, we generated nebulin-deficient mice by using a Cre knock-in strategy. Lineage studies utilizing this mouse model demonstrated that *nebulin* is expressed uniformly in all skeletal muscles. Nebulin-deficient mice die within 8–11 d after birth, with symptoms including decreased milk intake and muscle weakness. Although myofibrillogenesis had occurred, skeletal muscle thin filament lengths were up to 25% shorter compared with wild type, and thin filaments were uniform in length both within and between muscle types. Ultrastructural studies also demonstrated a critical role for nebulin in the maintenance of sarcomeric structure in skeletal muscle. The functional importance of nebulin in skeletal muscle function was revealed by isometric contractility assays, which demonstrated a dramatic reduction in force production in nebulin-deficient skeletal muscle.

Introduction

Nebulin is a giant modular sarcomeric protein (500–900 kD) in skeletal muscle, where it comprises ∼3% of total myofibrillar protein (Wang and Wright, 1988). A critical role for nebulin in skeletal muscle function is demonstrated by human mutations in *nebulin*, which are causative for nemaline myopathy, a neuromuscular disorder characterized by muscle weakness and the presence of rodlike nemaline bodies in the muscle fibers that contain abnormally arranged Z-line and I-band proteins (Wallgren-Pettersson et al., 1999, 2002). Nebulin has been proposed to be important for multiple aspects of striated muscle form and function (McElhinny et al., 2005). However, its exact role in vivo remains elusive.

Nebulin is encoded by a single gene, and its molecular weight ranges from 500 to 900 kD because of extensive isoform diversity in different muscle types, species, developmental stages, and in disease (Labeit and Kolmerer, 1995; Kazmierski et al., 2003; Donner et al., 2004). Single molecules of nebulin are associated with thin filaments in skeletal muscle and span the entire length of the thin filament with the COOH terminus anchored in the Z-line and the NH_2 terminus extending to the pointed end of the thin filaments (Wang and Wright, 1988; Millevoi et al., 1998; McElhinny et al., 2001). The molecular size of nebulin correlates with variations in thin filament lengths in different muscle types, suggesting that nebulin may act as a molecular ruler to regulate thin filament length in skeletal muscle (Labeit and Kolmerer, 1995; Wang, 1996). According to the cross-bridge theory of muscle contraction (Huxley and Simmons, 1971), the amount of force that a muscle can exert at different sarcomere lengths is determined by the amount of overlap between thin and thick filaments, which is dependent on thin filament length and the contractile state (Gordon et al., 1966; Granzier et al., 1991). In particular, thin filament lengths are fine tuned in different vertebrate muscles in vivo to overlap with thick filaments by an amount characteristic for each muscle such that the amount of force generated is suited to the physiological requirements for that muscle (Burkholder et al., 1994). Importantly, muscles working beyond their optimal length range, causing an incomplete overlap of thick and thin filaments, results in instability and damage (Morgan and Allen, 1999).

Correspondence to Ju Chen: juchen@ucsd.edu

X. Li's present address is Division of Cardiothoracic Surgery, University of California, San Diego, La Jolla, CA 92103.

Abbreviations used in this paper: EDL, extensor digitorum longus; ES, embryonic stem; PCSA, physiological cross-sectional area; SH3, Src homology 3; TA, tibialis anterior; TEM, transmission EM; VL, vastus lateralis.

The online version of this article contains supplemental material.

The Journal of Cell Biology, Vol. 173, No. 6, June 19, 2006 905–916
http://www.jcb.org/cgi/doi/10.1083/jcb.200603119

Nebulin might also play a role in myofibrillogenesis, where it appears to participate in the early assembly of precursor I-Z-I bodies, and assembles in a striated pattern before thin filaments attain their mature length (Moncman and Wang, 1996; Shimada et al., 1996; Nwe et al., 1999). This hypothesis is supported by a recent study showing the failure of myofibril assembly in cultured myotubes upon the knockdown of nebulin for 5 d (McElhinny et al., 2005). In addition, nebulin has been proposed to play a role in the regulation of muscle contraction by modulating actomyosin ATPase activity in a Ca^{2+}-calmodulin–dependent manner (Root and Wang, 1994, 2001).

Interactions of nebulin with diverse sarcomere-associated proteins suggest potential roles in sarcomeric architecture, signaling, and force transduction. Nebulin is composed mainly of ~35 amino acid modules (M1–185), which are further organized into super-repeats of seven modules within the central region of nebulin (M9–162). Each nebulin module interacts with a single actin monomer, and each super-repeat associates with each tropomyosin–troponin regulatory complex along the length of the thin filament (Jin and Wang, 1991; Pfuhl et al., 1994; Wang, 1996). Within the COOH-terminal region of nebulin, modules M163–170 interact with the intermediate filament desmin in the periphery of the Z-line, suggesting that nebulin might play a role in the lateral registration of sarcomeres and in force transmission (Bang et al., 2002). Nebulin's extreme COOH-terminal end contains a unique serine-rich domain with several potential phosphorylation sites and a Src homology 3 (SH3) domain, suggesting that nebulin might be involved in signaling pathways at the Z-line. The SH3 domain interacts with myopalladin, which, in turn, binds to α-actinin, thereby tethering nebulin at the Z-line (Bang et al., 2001; McElhinny et al., 2003). In addition, recent evidence suggests that nebulin's SH3 domain might also bind to the springlike PEVK domain in the I-band region of titin (Ma and Wang, 2002). In nebulin's NH_2-terminal region, modules M1–3 bind to the thin filament pointed end–capping protein tropomodulin (McElhinny et al., 2001), which is critical for maintaining thin filament length at the pointed ends (Littlefield et al., 2001; McElhinny et al., 2001). The interaction between nebulin and tropomodulin as well as a recent RNA interference study support the proposed function of nebulin as a regulator of thin filament length (McElhinny et al., 2005).

Nebulin was long thought to be absent from cardiac muscle, where the homologous but smaller protein nebulette is expressed (Moncman and Wang, 1995). However, recent studies have shown that *nebulin* is expressed in cardiac muscle and is localized in a layout identical to that in skeletal muscle, although at lower levels (Fock and Hinssen, 1999; Kazmierski et al., 2003; Donner et al., 2004; Joo et al., 2004). In addition, an RNA interference study in cardiomyocytes has suggested that nebulin is involved in thin filament length regulation in both cardiac and skeletal muscle (McElhinny et al., 2005). Based on this study, two distinct models have been proposed to explain how nebulin functions to regulate thin filament lengths in the heart (Fowler et al., 2006; Horowits, 2006).

As discussed above, multiple roles have been suggested for nebulin, including the regulation of thin filament length,

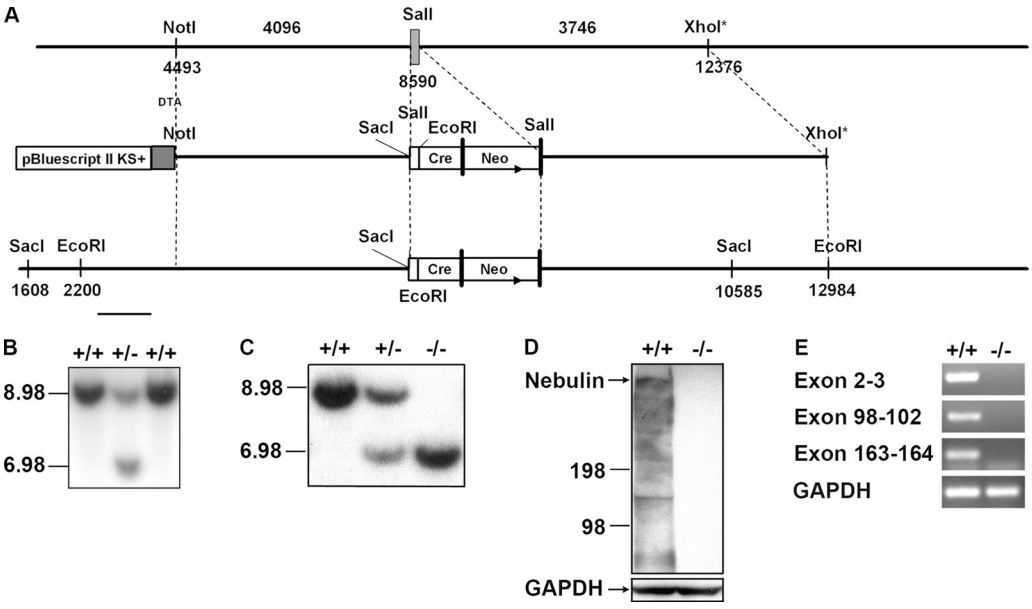

Figure 1. **Targeting of the *nebulin* gene.** (A) Targeting strategy. A restriction map of the relevant genomic region of *nebulin* is shown at the top, the targeting construct is shown in the middle, and the mutated locus after recombination is shown at the bottom. The grey box indicates exon 1, and black boxes indicate frt sites. DTA, Diphteria toxin A chain; Neo, neomycin resistance gene. (B) Detection of wild-type and targeted alleles by Southern blot analysis. DNA from electroporated ES cells was digested with SacI and analyzed by Southern blot analysis with a probe as shown in A. The 8.977- and 6.982-kb bands represent wild-type and targeted alleles, respectively. (C) Southern blot analysis of DNA isolated from postnatal day 1 wild-type, *nebulin*$^{+/-}$, and *nebulin*$^{-/-}$ mice. DNA was digested with SacI and analyzed by Southern blot analysis with the probe shown in A. (D) Detection of nebulin protein by Western blot analysis. Protein prepared from postnatal day 1 skeletal muscle of wild-type and *nebulin*$^{-/-}$ mice was analyzed with antinebulin M161–165 and anti–glyceraldehyde-3-phosphate dehydrogenase (GAPDH) monoclonal antibodies. (E) RT-PCR using primers for exons 2 and 3, 98–102, and 163 and 164 confirmed that nebulin was successfully knocked out.

myofibrillogenesis, signal transduction, regulation of muscle contraction, and myofibrillar force generation. However, requirements for nebulin in vivo have not yet been addressed. To study the functional role of nebulin in vivo, we generated nebulin-deficient mice by using a Cre knockin approach. This strategy also allowed us to study the endogenous expression pattern of *nebulin* by crossing these mice with Rosa26 lineage reporter mice (Soriano, 1999). Our lineage studies revealed that *nebulin* is expressed in all skeletal muscle myocytes. *Nebulin* expression was also identified in the heart. However, *nebulin* was shown to be expressed mainly in the atria, where it was expressed heterogeneously in ~50% of atrial cardiomyocytes, whereas it was expressed only in a minor percentage of ventricular cardiomyocytes. These results suggest that nebulin may have a more critical role in skeletal muscle than in cardiac muscle.

Nebulin-deficient mice die within 8–11 d after birth, with symptoms including decreased milk intake and muscle weakness. Transmission EM (TEM) and immunostaining analyses demonstrated that nebulin is not important for the normal assembly of sarcomeres. However, nebulin-deficient mice had skeletal muscle thin filaments that were decreased in length by up to 25% compared with wild type. Also, thin filaments were uniform in length both within and between muscle types. This is in contrast to a recent study (McElhinny et al., 2005) in cultured cardiomyocytes in which the RNA interference knockdown of nebulin resulted in a 30% increase in thin filament lengths. Our analyses further indicate a critical role for nebulin in the maintenance of sarcomere structure and demonstrate a dramatic reduction in force production by nebulin-deficient skeletal muscle.

Results

Generation of *nebulin*-deficient mice

To study the function and expression pattern of *nebulin* in vivo, we generated *nebulin*-deficient mice by gene targeting. Exon 1 was deleted and replaced by *Cre* recombinase cDNA as well as the neomycin resistance gene flanked by frt sites (Fig. 1 A). After electroporation of the targeting vector into R1 embryonic stem (ES) cells, one clone was identified that had undergone homologous recombination (Fig. 1 B). The clone was injected into blastocysts from C57/B6 mice and gave rise to chimera mice that were then bred with Black Swiss mice to generate germ line–transmitted heterozygous *nebulin*$^{+/-}$ mice. These mice were subsequently mated to generate homozygous *nebulin*$^{-/-}$ mice. To verify that homozygous knockout mice were null mutants, we performed Southern blot analysis on DNA isolated from *nebulin*$^{-/-}$ and *nebulin*$^{+/-}$ mice (Fig. 1 C) as well as Western blot analyses for nebulin protein using a polyclonal antibody raised against domain M161–165. As shown in Fig. 1 D, no nebulin protein was detected in *nebulin*$^{-/-}$ mice. In addition to the high molecular mass band at nebulin's expected size, lower molecular mass bands of ~130 and 60 kD were detected that were also absent in *nebulin*$^{-/-}$ mice. This could either be alternative splice isoforms of nebulin or degradation products from the lysate preparation, which has also been seen in other studies using various antibodies (Kazmierski et al., 2003; McElhinny et al., 2005). We also performed RT-PCR analysis on RNA isolated from gastrocnemius muscle using primers located in exons 2, 3, 98–102, 163, and 164 (mouse *nebulin* has 165 exons; Kazmierski et al., 2003), which suggested that the entire nebulin was successfully knocked out (Fig. 1 E).

Nebulin is uniformly expressed in skeletal muscle

Nebulin$^{+/-}$ mice were viable and indistinguishable from their wild-type littermates. To determine the expression pattern of endogenous *nebulin* in vivo, *nebulin*$^{+/-}$ mice were crossed with the Rosa26 lineage reporter mouse (Soriano, 1999). In the progeny of this cross, Cre-mediated excision at the Rosa26 locus results in the expression of the β-galactosidase (lacZ) gene under the control of the ubiquitously expressed Rosa26 locus, thus allowing lineage analysis of nebulin-expressing cells. Various tissues from 10-wk-old *nebulin*$^{+/-}$ Rosa26 mice were fixed and stained with X-galactosidase. As expected, strong β-galactosidase

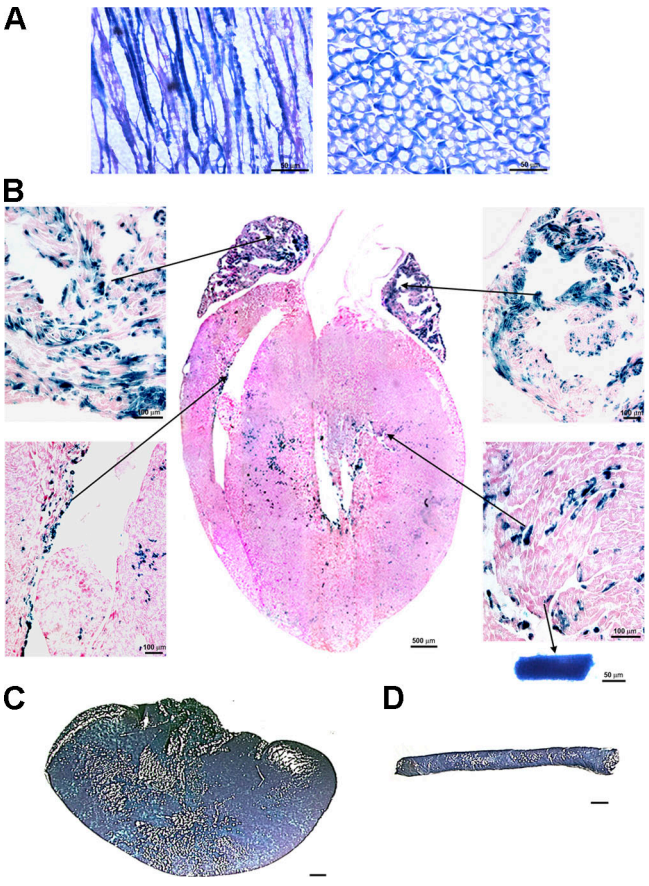

Figure 2. ***Nebulin* is expressed in skeletal and cardiac muscle.** X-galactosidase staining of tissue from *nebulin*$^{+/-}$ Rosa26 mice. (A) X-galactosidase staining of heart sections reveals *nebulin* expression mainly in atrial cardiomyocytes and only in a small percentage of ventricular cardiomyocytes. Enlarged images of different areas from the heart are shown (arrows refer to the enlarged areas). (B) X-galactosidase staining of heart sections reveals *nebulin* expression mainly in atrial cardiomyocytes and only in a small percentage of ventricular cardiomyocytes. (bottom right) LacZ-positive cardiomyocyte. (C and D) X-galactosidase staining was also positive for the liver (C) and aorta (D). Bars (C and D), 1 mm.

activity was detected homogenously in all skeletal muscle types (Fig. 2 A). In addition, β-galactosidase expression was detected in the heart, aorta, and liver (Fig. 2, B–D). No β-galactosidase activity was detected in other tissues. Because the presence of *nebulin* in the heart has only recently been reported (Fock and Hinssen, 1999; Kazmierski et al., 2003; Donner et al., 2004; Joo et al., 2004) and has not yet been thoroughly characterized, we further examined its expression pattern in the heart. X-galactosidase staining of frozen sections from the heart revealed that *nebulin* is expressed mainly in the left and right atria (~50% of cardiomyocytes), whereas in the ventricles, *nebulin* is expressed only in a small percentage of cardiomyocytes (Fig. 2 B).

Nebulin-deficient mice die at postnatal day 8–11

Nebulin$^{-/-}$ mice were born in Mendelian ratios with a similar body weight compared with their wild-type littermates. *Nebulin*$^{-/-}$ mice were able to breathe and move their legs and were indistinguishable from their wild-type littermates except that *nebulin*$^{-/-}$ mice had little or no detectable milk in their stomachs, presumably reflecting an inability to suckle. Consistent with this observation, *nebulin*$^{-/-}$ mice barely increased in weight after birth and exhibited minimal subcutaneous fat. *Nebulin*$^{-/-}$ mice died ~8–11 d after birth with a weight ~25% of that of their wild-type littermates, which was most likely the result of decreased milk intake caused by muscle weakness (Fig. 3, A and B). Because *nebulin*$^{-/-}$ mice were able to survive up until 11 d, we assumed that they were able to drink some milk. Therefore, we tested whether *nebulin*$^{-/-}$ mice would be able to survive longer in the absence of competition from wild-type littermates by removing wild-type littermates after birth. However, this had no effect on the size or lifespan of the *nebulin*$^{-/-}$ mice.

Histological analysis by hematoxylin and eosin staining of frozen sections of skeletal and heart muscle from postnatal day 1 mice showed no obvious differences between *nebulin*$^{-/-}$ and wild-type mice (unpublished data). No fibrosis was detected by trichrome staining of either skeletal or heart muscle from *nebulin*$^{-/-}$ mice (unpublished data). We also analyzed myosin heavy chain composition in several distinct skeletal muscles by gel electrophoretic analyses and observed no differences between mutant and wild-type mice (unpublished data). Both had prominent neonatal and embryonic myosin heavy chain bands that were consistent with previous findings (Agbulut et al., 2003).

Nebulin$^{-/-}$ mice have normal myofibrillogenesis but exhibit sarcomeric misalignment and disorganization after muscle usage

To determine the structure of skeletal muscle in more detail, TEM analysis was performed on tibialis anterior (TA) muscle from 1-d-old *nebulin*$^{-/-}$ and littermate control mice. Postnatal day 1 was chosen because *nebulin*$^{-/-}$ and wild-type littermate mice were still similar in size at this stage, thus facilitating a valid comparison. To allow us to study the ultrastructure of TA muscle at different sarcomere lengths, legs were fixed with the

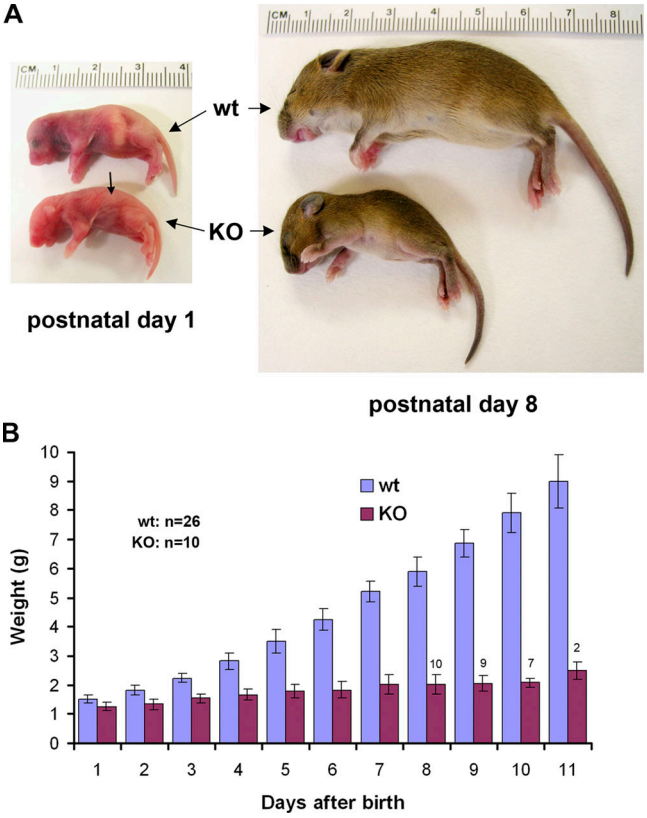

Figure 3. ***Nebulin*$^{-/-}$ mice are born at a similar weight as their wild-type littermates but die at postnatal day 8–11 at a weight ~25% of that of their wild-type littermates.** (A) *Nebulin*$^{-/-}$ (knockout; KO) mice at postnatal days 1 and 8 as compared with wild-type (wt) littermate controls. (B) Typical growth of *nebulin*$^{-/-}$ (KO) mice compared with wild-type littermate control mice from postnatal day 1–11 when *nebulin*$^{-/-}$ mice die. No statistical differences between wild-type and *nebulin*$^{+/-}$ pups were observed. Numbers above the bars for *nebulin*$^{-/-}$ mice indicate the number of remaining viable mice. Error bars represent SEM.

knee joint at 90° and with the ankle at 90° (neutral) or 180° (fully plantarflexed), as plantarflexion of the ankle joint causes stretching of the TA muscle.

At resting length, muscles from *nebulin*$^{-/-}$ mice had relatively normal sarcomeric structure with wide myofibrils, distinct A-bands, and narrow, uniformly spaced Z-lines (Fig. 4, A and B), suggesting that sarcomere assembly and organization were preserved in the absence of nebulin. However, the misalignment of myofibrils was often observed. In moderately stretched muscle, myofibrillar misalignment was more pronounced (Fig. 4, C–F), and myofibril splitting frequently appeared. In addition, fragmented Z-lines were apparent, whereas M-lines appeared unaffected. Similar results were obtained by TEM of muscle tissue from *nebulin*$^{-/-}$ mice at postnatal day 6 (unpublished data).

To determine whether the observed ultrastructural abnormalities in *nebulin*$^{-/-}$ muscle resulted from abnormal sarcomere assembly or an inability to maintain myofibrillar integrity during muscle contraction, we compared embryonic and postnatal diaphragm muscle in *nebulin*$^{-/-}$ mice with littermate controls. Diaphragm muscle remains inactive during embryogenesis, thus allowing a determination of whether nebulin is required for myofibrillogenesis before the onset of contraction. After birth,

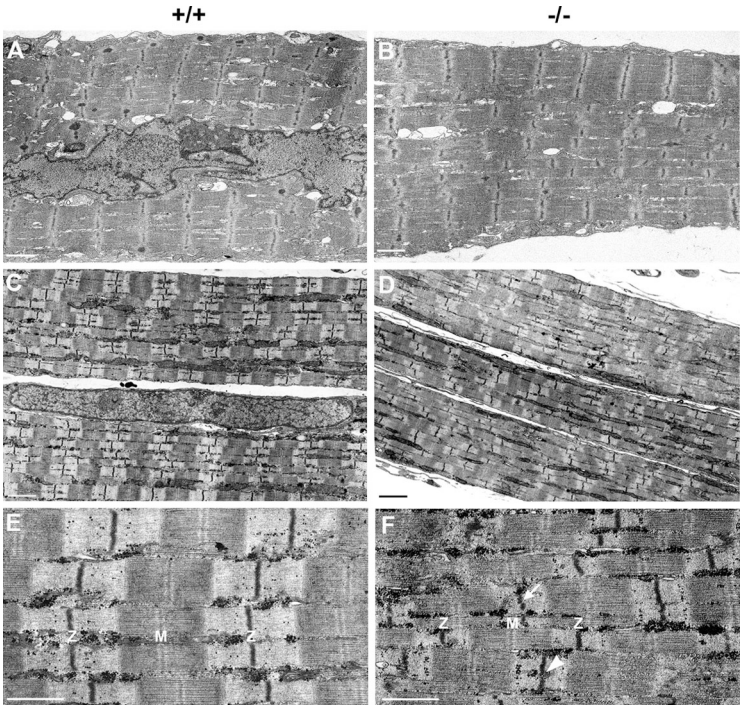

Figure 4. **TEM of TA muscle from *nebulin*$^{-/-}$ mice at postnatal day 1.** TEM of relaxed TA muscle from wild-type (A) and *nebulin*$^{-/-}$ mice (B) showed relatively normal sarcomeric organization in *nebulin*$^{-/-}$ mice, although some sarcomeres were misaligned. TEM of stretched TA muscle from wild-type (C and E) and *nebulin*$^{-/-}$ mice (D and F) revealed myofibrillar misalignment with evidence of myofibril splitting (arrowhead) and fragmentation of Z-lines (arrow) in *nebulin*$^{-/-}$ mice. M, M-line; Z, Z-line. Bars, 1 μm.

the diaphragm is continuously contracting and, therefore, is useful for studying the requirement for nebulin in actively contracting muscle.

At embryonic day 18.5, *nebulin*$^{-/-}$ diaphragm muscle had well-aligned sarcomeres that were virtually indistinguishable from those of wild-type muscle (Fig. 5, A and B). At postnatal

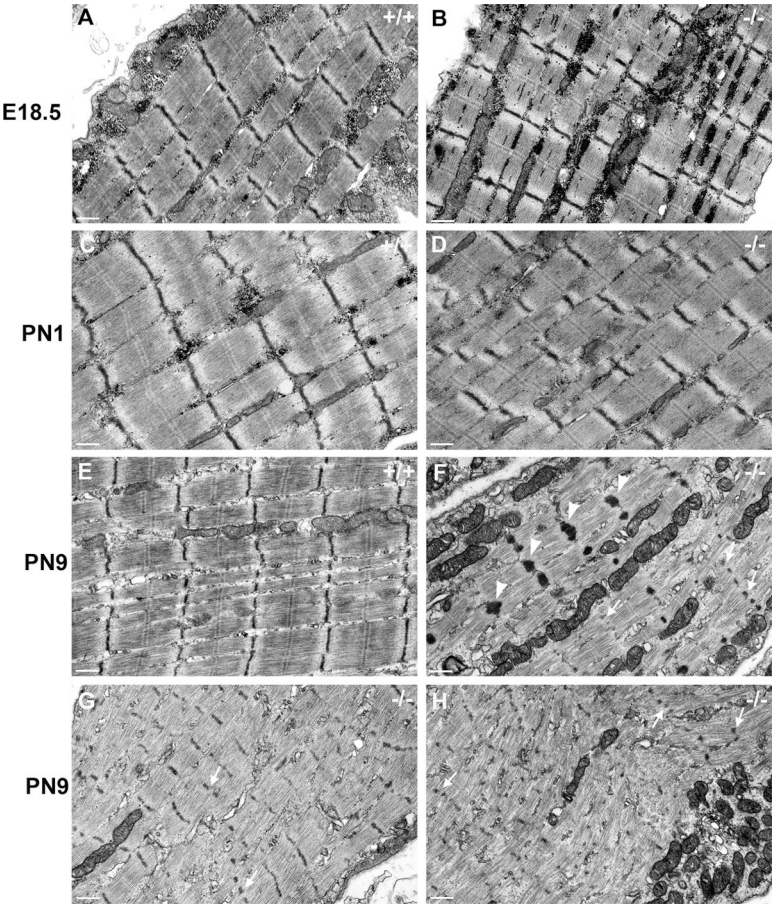

Figure 5. **TEM of diaphragm muscle.** Micrographs of longitudinal sections of diaphragm muscle from wild-type (A, C, and E) and *nebulin*$^{-/-}$ mice (B, D, F, G, and H) at embryonic day (E) 18.5 (A and B), postnatal day (PN) 1 (C and D), and postnatal day 9 (E–H). In the noncontracting diaphragm at embryonic day 18.5, *nebulin*$^{-/-}$ mice showed normal sarcomeric organization with well-aligned sarcomeres (B) and were comparable with wild-type muscle (A). At postnatal day 1, *nebulin*$^{-/-}$ mice exhibited misaligned sarcomeres with moderately wider Z-lines compared with wild type (C and D). By postnatal day 9, myofibril architecture was severely disrupted (F–H) with either thick (arrowheads in F), punctate (arrows in F–H), or dissolving Z-lines (G and H). In addition, M-lines became poorly defined, and abnormal accumulations of mitochondria were present. Bars, 500 nm.

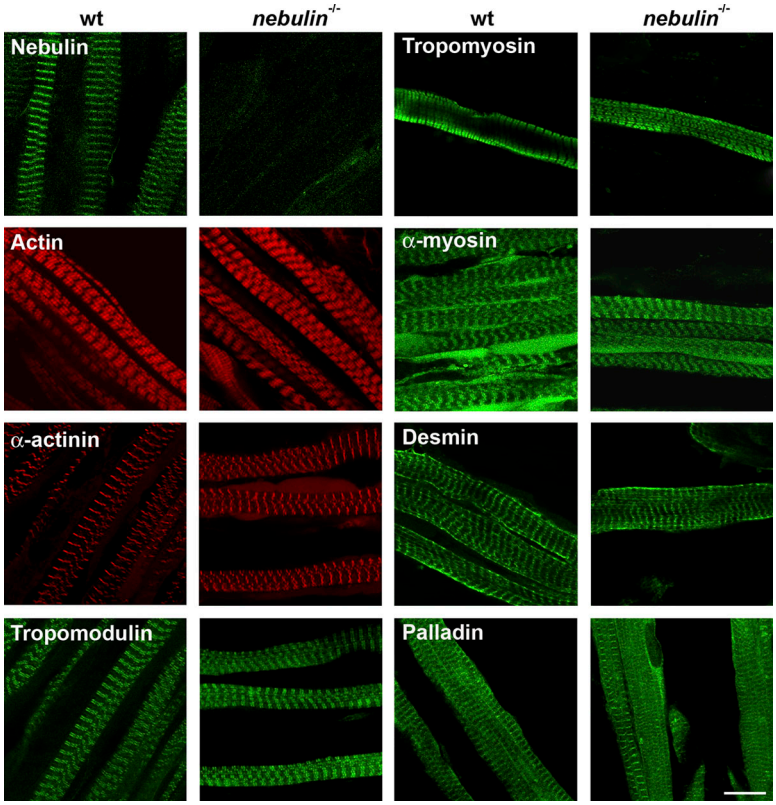

Figure 6. **Immunolabeling with antibodies against various cytoskeletal proteins.** Immunostaining of frozen sections from the TA muscle stained for nebulin, actin (phalloidin), α-actinin, tropomyosin, tropomodulin, α-myosin, desmin, and palladin. Bar, 10 μm.

day 1, the misalignment of myofibrils and moderate thickening of Z-lines were observed in diaphragm muscle from *nebulin*$^{-/-}$ mice (Fig. 5 D). At postnatal day 9, *nebulin*$^{-/-}$ diaphragm muscle exhibited a severe disruption of myofibrillar structure, including a lack of well-defined A- and I-bands (Fig. 5, F–H). Z-lines exhibited various types of morphologies. Some Z-lines were extremely thick, rounded, and highly electron dense, resembling nemaline rod bodies (Fig. 5 F; Wallgren-Pettersson et al., 1999, 2002), whereas others were punctate and appeared fragmented (Fig. 5, F–H). Moreover, some fibers exhibited a complete lack of organization with Z-lines that appeared to be dissolving (Fig. 5 H). Another interesting observation was the abnormal accumulation of mitochondria within myofibers (Fig. 5 H). These observations suggest that nebulin is not required for myofibrillogenesis but is important for the maintenance of myofibrillar integrity during muscle contraction.

Nebulin$^{-/-}$ mice have normally assembled sarcomeric components

To determine how the ablation of nebulin affected other cytoskeletal proteins, we stained TA and extensor digitorum longus (EDL) muscles from 1-d-old *nebulin*$^{-/-}$ mice and littermate controls for α-actinin 2, α-myosin, actin (phalloidin), tropomodulin, tropomyosin, desmin, and palladin (Fig. 6), many

Table I. **Thin filament measurements in skeletal muscle from *nebulin*$^{-/-}$ and wild-type mice**

Muscle	Probe	Wild type			*nebulin*$^{-/-}$			Wild-type *nebulin*$^{-/-}$		
		Length	Range	*n*	Length	Range	*n*	ΔLength	Percentage of wild type	P value
		μm			μm			μm		
Gast	Tmod	1.27 ± 0.06	1.11–1.35	26	0.95 ± 0.04	0.85–1.06	41	0.318	25	5.68E-24
VL	Tmod	1.29 ± 0.05	1.19–1.38	13	1.05 ± 0.06	0.97–1.19	21	0.241	19	7.60E-14
TA	Tmod	1.29 ± 0.05	1.19–1.39	32	1.07 ± 0.07	0.91–1.17	29	0.213	17	3.45E-19
EDL	Tmod	1.16 ± 0.06	1.01–1.31	60	1.04 ± 0.07	0.89–1.20	25	0.123	11	2.03E-09
TA	Phall	1.17 ± 0.02	1.14–1.20	4	0.95 ± 0.05	0.90–1.07	15	0.221	19	5.33E-08
Total				135			131			

Tmod, tropomodulin; Phall, phalloidin; Gast, gastrocnemius. Note that calculations based on phalloidin staining generally resulted in shorter thin filament lengths in both wild-type and *nebulin*$^{-/-}$ mice, which is likely to be the result of systematically shorter thin filament lengths estimated by the Gaussian distribution that was used to estimate the microscope point spread function (Littlefield et al., 2001). However, in TA muscle stained with phalloidin, distributed deconvolution analysis revealed a 0.22-μm decrease in thin filament length in the absence of nebulin, which is similar to the observed decrease of 0.21 μm that was measured based on α-actinin and tropomodulin costainings.

of which have been shown to interact with nebulin. Although *nebulin*$^{-/-}$ sarcomeric structure was less well organized compared with wild-type control mice, no obvious differences in the localization of any of these proteins were found. We also assessed the localization of these proteins at postnatal day 8 before the death of *nebulin*$^{-/-}$ mice and found no significant changes (unpublished data). Thus, nebulin is not critical for normal sarcomere assembly or the localization of several sarcomeric proteins.

Nebulin$^{-/-}$ mice have reduced thin filament lengths compared with wild type

Because nebulin has been proposed to play a role in the regulation of thin filament length, we examined thin filament lengths in *nebulin*$^{-/-}$ mice. In *nebulin*$^{-/-}$ mice, tropomodulin was localized in its typical striated pattern at the pointed ends of the thin filaments and was expressed in similar amounts compared with wild type as assessed by Western blot analysis (unpublished data). Thus, we measured thin filament lengths either by double immunostaining for α-actinin and tropomodulin, which stain Z-lines and thin filament pointed ends, respectively, or by fluorescently labeled phalloidin to directly localize thin filaments. Stained samples were analyzed by distributed deconvolution, which determines the location, brightness, and dimensions of each thin filament array (I-Z-I body) along a myofibril at subpixel resolution and is independent of sarcomere length differences (Littlefield and Fowler, 2002).

Using distributed convolution on α-actinin– and tropomodulin-stained muscle sections, we measured thin filament lengths in four different muscles from wild-type and *nebulin*$^{-/-}$ mice: gastrocnemius, TA, vastus lateralis (VL), and EDL (Table I). In addition, our results were independently verified by phalloidin staining for TA muscle. A total of three wild-type and three *nebulin*$^{-/-}$ mice were used for the analysis. Examples of the analysis on TA and gastrocnemius muscle are shown in Fig. 7 and as supplemental data (Fig. S1, available at http://www.jcb.org/cgi/content/full/jcb.200603119/DC1), respectively. As shown in Table I, the absence of nebulin resulted in a significant shortening of thin filament lengths by 0.07–0.28 μm in all four muscle types examined. Intriguingly, the absence of nebulin resulted in similar thin filament lengths of ∼0.95–1.07 μm in all four muscles (Table I), whereas in wild-type muscle, thin filaments lengths were 1.27 ± 0.06, 1.29 ± 0.05, 1.29 ± 0.05, and 1.16 ± 0.06 μm in gastrocnemius, VL, TA, and EDL muscle, respectively. Thus, gastrocnemius, VL, and TA thin filaments were shortened the most (0.28, 0.25, and 0.21 μm, respectively), whereas EDL thin filaments, which were the shortest in wild-type mice, only shortened by 0.07 μm in the *nebulin*$^{-/-}$ mice.

Nebulin$^{-/-}$ skeletal muscle generates significantly lower stress compared with wild type

To determine the functional effects of the ultrastructural changes in the *nebulin*$^{-/-}$ mice, we measured force production. At postnatal day 1, TA muscle in *nebulin*$^{-/-}$ mice were grossly indistinguishable from wild-type littermates (Fig. 8 A, inset). However, the neonatal tendon was translucent and mechanically fragile,

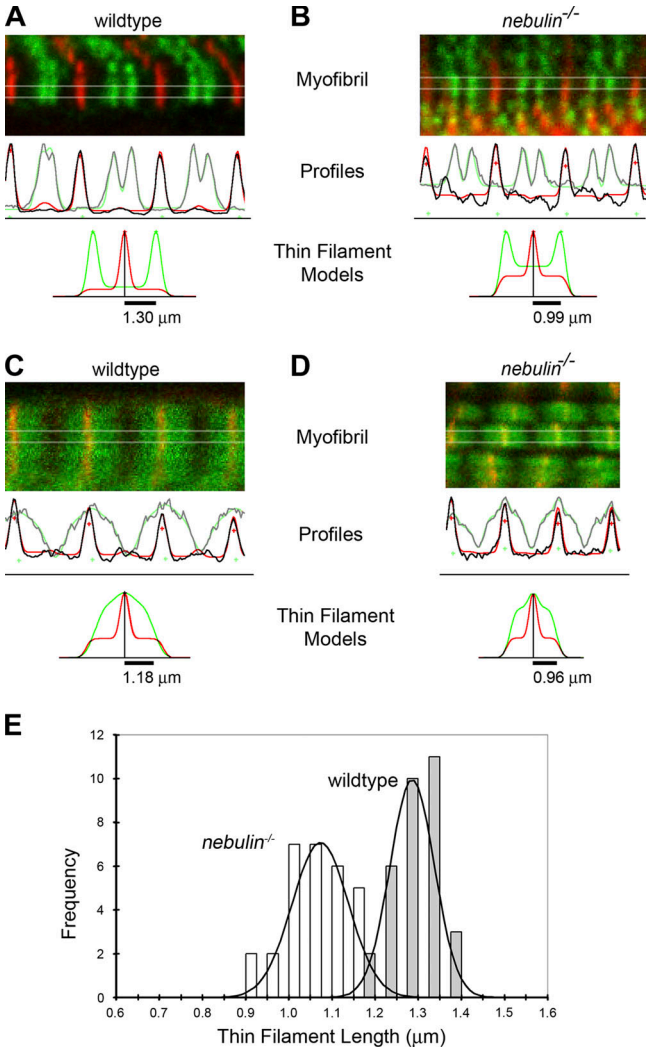

Figure 7. **Thin filament lengths in TA muscle from *nebulin*$^{-/-}$ mice are shorter compared with wild-type mice.** Myofibril image regions, line scan profiles, and thin filament models for wild-type (A) and *nebulin*$^{-/-}$ (B) mice stained for α-actinin (red) and tropomodulin (green) or for wild-type (C) and *nebulin*$^{-/-}$ (D) mice stained for α-actinin (red) and phalloidin (green). Myofibrils: the regions used for each line scan are indicated on each image by a semitransparent overlay. Image regions above and below the line scan region were used to calculate background values. Profiles: optimized intensity fits for α-actinin (red) and either tropomodulin or phalloidin (green) closely fit the line scan intensity values (gray and black lines). Thin filament models: individual α-actinin (red) and either tropomodulin or phalloidin (green) model distributions optimized to fit the observed line scan intensities by repeating each profile along the length of the line scan for each Z-line. Thin filament lengths determined by the tropomodulin or phalloidin peaks are indicated below the profiles. (B) Histogram of thin filament lengths measured for wild-type and *nebulin*$^{-/-}$ mice. Curves show the Gaussian fit to the data.

making it difficult to test contractile force in *nebulin*$^{-/-}$ mice using traditional techniques. As a result, isometric contractile testing of the isolated TA bone–tendon–muscle–tendon–bone complex was performed using high resolution force transducers to yield a signal to noise ratio of >20 (Fig. 8 A). A total of 16 TA muscles from wild-type and 9 from *nebulin*$^{-/-}$ mice were used for the analysis. Electrophysiological threshold contractile kinetics were similar between *nebulin*$^{-/-}$ and wild-type mice, which suggested that excitation/contraction coupling was not significantly altered in *nebulin*$^{-/-}$ mice (unpublished data). However,

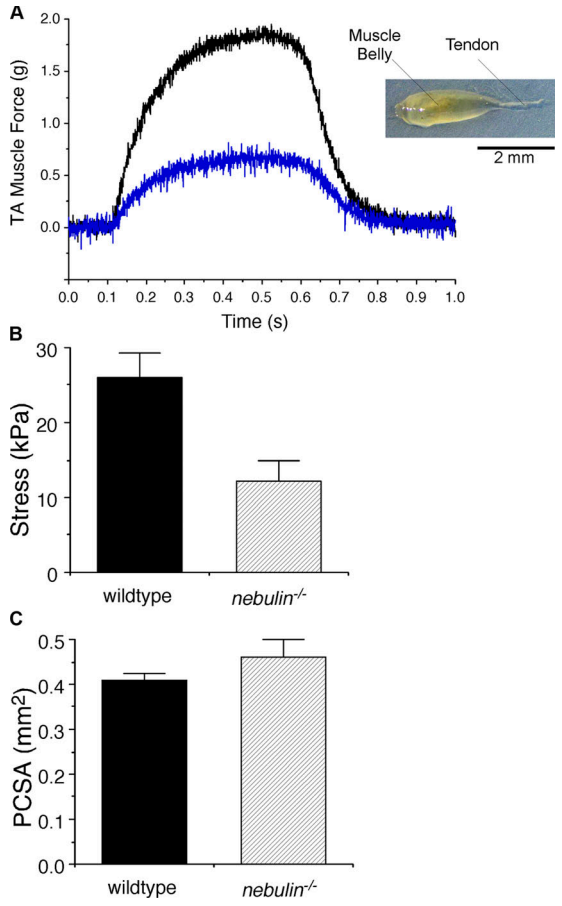

Figure 8. **Contractile properties of 1-d-old muscles.** (A) Isometric contractile properties of mouse TA muscle (inset) from wild-type (black) and *nebulin*$^{-/-}$ mice (blue). Note the decreased force generated over a similar time course. This implicates the force-generating/transmitting system. (B) Stress generated by wild-type (black) and *nebulin*$^{-/-}$ (hatched) muscles. Note that the *nebulin*$^{-/-}$ muscles generate <50% of the wild-type stress ($P < 0.001$). (C) Physiological cross-sectional area (PCSA) of wild-type (black) and *nebulin*$^{-/-}$ (hatched) muscles. See Materials and methods for the definition of PCSA. The PCSA of the two genotypes is nearly identical, demonstrating that both muscles have the same amount of force-generating material, but the *nebulin*$^{-/-}$ muscle is of inferior quality, thus explaining the lower stress (see B). Data is presented as mean ± SEM (error bars) for wild-type ($n = 14$) and *nebulin*$^{-/-}$ ($n = 9$) muscles.

the magnitude of the stress generated by *nebulin*$^{-/-}$ mice was <50% of the wild-type value (Fig. 8 B). Overall stress generated by neonatal muscle was 5–10% that of adult mammalian muscle, probably because of the fact that the myofibrils were less dense (Fig. 3). It is important to note that the low stress was not simply because *nebulin*$^{-/-}$ TA muscles were smaller since there was no significant difference between the physiological cross-sectional area (PCSA; Fig. 8 C) of TA muscles. Thus, the force transmission efficiency of the contractile complex of the *nebulin*$^{-/-}$ mouse was critically compromised even though the contractile machinery appeared to be of normal morphology (Fig. 5) and fiber size between the two genotypes was similar (not depicted).

Discussion

To determine the functional role of nebulin in vivo, we generated mice deficient for nebulin. *Nebulin* exon 1 was replaced by a Cre-neo cassette, thereby knocking out *nebulin*. Successful ablation of the entire *nebulin* was confirmed by DNA, RNA, and protein analysis. The presence of Cre in the targeting allele allowed us to examine cells in which *nebulin* is/has been expressed by crossing *nebulin*$^{+/-}$ mice with the Rosa26 reporter line. As expected, this revealed a strong and uniform expression of *nebulin* in all types of skeletal muscle. In addition, we confirmed the recently reported nebulin expression in cardiac muscle (Fock and Hinssen, 2002; Kazmierski et al., 2003; Donner et al., 2004; Joo et al., 2004). However, *nebulin* was primarily expressed in the atria (~50% of atrial cardiomyocytes) and only in a small percentage of ventricular cardiomyocytes, predominantly in the inner layer of the myocardium. Further studies are needed to elucidate the potential functions of nebulin in the heart as well as in other sites of expression.

Nebulin is critical for survival in mice

Our study shows that nebulin is critical for mouse survival because the genetic ablation of *nebulin* caused death with complete penetration in neonatal mice from postnatal day 8–11. Lethality may be caused by several factors. The reduced milk intake and impaired growth observed in *nebulin*$^{-/-}$ mice suggest that these mice may have difficulties in suckling, presumably as a result of decreased muscle function. This is supported by our ultrastructural and biophysical studies demonstrating abnormal sarcomeric structure and severely reduced force generation in skeletal muscle of *nebulin*$^{-/-}$ mice. Thus, starvation as a result of reduced suckling may contribute to death. Because severely disorganized diaphragm muscle structure was also observed in postnatal *nebulin*$^{-/-}$ mice, impaired breathing caused by defective diaphragm muscle may also cause lethality.

Nebulin$^{-/-}$ is not required for myofibrillogenesis but is essential for the maintenance of myofibrillar integrity during muscle contraction

Our ultrastructural observations in embryonic day 18.5 diaphragm muscle demonstrated that nebulin is not essential for myofibrillogenesis. In addition, immunostaining analyses demonstrated that nebulin is not required for the association of several sarcomeric proteins with the sarcomere, including tropomodulin. Whereas *nebulin*$^{-/-}$ diaphragm muscle displayed a mild misalignment of myofibrils and moderate thickening of Z-lines at postnatal day 1 when the diaphragm had recently started to contract, diaphragm muscle was severely disorganized at postnatal day 9. This suggests that nebulin is essential for the maintenance of muscle integrity during contraction. Compared with TA muscle at postnatal days 1 and 6, diaphragm muscle was much more severely affected, likely because of the constant stress during the continuous contraction of diaphragm muscle. Interestingly, the thickening of Z-lines and the presence of rod-like nemaline bodies in diaphragm muscle at postnatal day 9 is reminiscent of observations in patients with nemaline myopathy (Wallgren-Pettersson et al., 1999, 2002). We are not sure of the composition of these enlarged Z- lines, but based on the characterization of nemaline rod bodies from nemaline myopathy patients, we predict that they may represent an accumulation of

Z- and I-band components (Wallgren-Pettersson et al., 2002). Several of the observed abnormalities at postnatal day 9 are likely to be secondary to prolonged muscle malfunction, which appear to initiate with myofibril misalignment and loss of Z-line integrity and eventually lead to the dissolution of muscle structure.

Nebulin is required to specify thin filament length in a muscle-specific manner

Because nebulin has long been proposed to function as a ruler for specifying thin filament length and fit into many of the criteria that could be expected from a molecular ruler, one of our main aims was to determine the effect of nebulin deficiency on thin filament length in skeletal muscle. Intriguingly, individual muscles in *nebulin*$^{-/-}$ mice had thin filaments that were uniform in length but up to 25% shorter compared with wild type. Also, whereas in wild-type mice, thin filament lengths varied between different muscle types, *nebulin*$^{-/-}$ mice had almost uniform thin filament lengths ($\sim$0.95–1.07 μm) among the four muscle types examined.

In contrast to our findings, a recent siRNA *nebulin* knockdown study performed in cultured cardiomyocytes resulted in the absence of localized tropomodulin and a 30% increase in thin filament lengths (McElhinny et al., 2005). Discrepancies between our findings and those of McElhinny et al. (2005) could reflect differences in the systems being used: cardiac versus skeletal, rat versus mouse, or in vivo versus in vitro. Because *nebulin* is only expressed in a small percentage of mouse ventricular myocytes, whereas it is uniformly expressed in all skeletal muscle cells, we performed our thin filament length measurements in skeletal muscle.

Nebulin-deficient mice had uniform thin filament lengths of $\sim$1 μm in all muscles tested, so a nebulin-independent mechanism must be responsible for specifying thin filament length in the absence of nebulin (Littlefield and Fowler, 1998). This supports a model in which a nebulin-independent mechanism defines uniform thin filament lengths of $\sim$1 μm in all muscle types, whereas nebulin is responsible for specifying longer thin filament lengths in a muscle-specific manner, thereby allowing individual muscles to fulfill specific physiological requirements. This is consistent with previous studies showing a correlation between the molecular size of nebulin and thin filament length (Labeit and Kolmerer, 1995; Wang, 1996). Thus, the expression of distinct *nebulin* isoforms in different muscles may be correlated with thin filament lengths in individual skeletal muscle types.

Nebulin is essential for efficient force transmission

TEM of *nebulin*$^{-/-}$ TA and diaphragm muscle revealed sarcomeric misalignment and various degrees of Z-line streaming and fragmentation, which was apparent from postnatal day 1 and increased with age. Although our immunofluorescence data showed that desmin is localized in its normal pattern in the periphery of the Z-line (Fig. 6), a possible explanation for the observed myofibrillar misalignment and Z-line streaming could be the missing linkage between desmin and the Z-line via nebulin. Disruption of the attachment of desmin in the Z-line could result in the loss of the lateral alignment of sarcomeres and less efficient force transmission. Intriguingly, active stress generation in *nebulin*$^{-/-}$ mice was $<$50% compared with wild-type controls. Similarly, stress generation in desmin-deficient mice was shown to be reduced by $\sim$20% (Sam et al., 2000). Thus, the mechanical relationship between nebulin and desmin might have dramatic consequences for force transmission in muscle, and nebulin is likely to play a role in transmitting the force from the thin filament to the intermediate filament system via desmin. The reduction in thin filament lengths would also be expected to reduce force generation as a result of decreased overlap between thin and thick filaments (Gordon et al., 1966) and/or limit the working range of the muscle (Burkholder et al., 1994). In addition to reduced force transmission, a possible mechanistic explanation for decreased muscle stress could be the increased sarcomeric heterogeneity and misalignment observed in *nebulin*$^{-/-}$ mice. The significant change in active stress is likely to be a reflection of several of these factors.

Conclusions

In conclusion, our studies have demonstrated that nebulin is not required for myofibrillogenesis. However, nebulin is important for muscle stability, organization, and force generation in vivo. In addition, we have demonstrated that nebulin is required to specify distinct thin filament lengths in individual skeletal muscle types, suggesting that the specificity of thin filament length within individual muscle types may be dictated by the expression of specific nebulin isoforms. Variable thin filament lengths between different muscle types may reflect intrinsic functional requirements. Intriguingly, thin filament lengths in the absence of nebulin were uniform within and between individual muscle types and were consistently shorter in *nebulin*$^{-/-}$ mice, suggesting that thin filament length must be specified by another mechanism in the absence of nebulin. This is also indicated by the absence of nebulin in invertebrate striated muscle. The identification of this alternative mechanism for thin filament length regulation will be an interesting subject for further studies.

Materials and methods

Gene targeting and generation of *nebulin*-deficient mice

Nebulin genomic DNA was isolated from a 129SVJ mouse genomic library (Stratagene) and was used to construct a *nebulin*-targeting construct for the replacement of *nebulin* exon 1 by the *Cre* recombinase cDNA and the *neomycin* resistance gene. The construct was generated in the pBluescript II KS+ vector, and the 5′ arm of homology consisted of a 4.096-kb NotI–SalI fragment upstream of *nebulin* exon 1 fused in frame with *Cre* followed by *neomycin* flanked by *FRT* sites. The 3′ arm of homology was a 3.736-kb SalI–XhoI fragment located downstream of exon 2 (Fig. 1 A). The targeting construct was verified by sequencing and linearized with NotI before electroporation into R1 ES cells at the Transgenic Core Facility at the University of California, San Diego. 1,000 G418-resistant ES clones were screened for homologous recombination by Southern blot analysis as described in the next section.

Southern blot analysis

Genomic DNA was extracted from G418-resistant ES cell clones and mouse tails as previously described (Chen et al., 1998). ES cell DNA was digested with SacI and analyzed by Southern blot analysis. A 507-bp fragment corresponding to 2,676–3,182 kb of the target vector (indicated in Fig. 1 A) was generated by PCR using mouse genomic DNA and specific *nebulin* primers (forward, CGTGTGAGGATTGGAGGTTT; reverse, AGTGCATCACAGGGGTAAGG). The PCR product was subsequently radiolabeled

using α-[^{32}P]dATP by random priming (Invitrogen). DNA blots were hybridized with the radiolabeled probe and visualized by autoradiography. The wild-type allele is represented by a band of 8.977 kb, whereas a band of 6.982 kb represents the correctly targeted mutant allele.

Generation and genotyping of mice

One independent homologous recombinant ES clone was microinjected into blastocysts from C57/B6 mice at the Transgenic Core Facility at the University of California, San Diego. Male chimeras were inbred with female Black Swiss mice to generate germ line–transmitted heterozygous mice (*nebulin*$^{+/-}$). *Nebulin*$^{+/-}$ mice were subsequently intercrossed to generate mice, which were homozygous null mutant mice (*nebulin*$^{-/-}$).

Offspring from intercrosses were genotyped by PCR analysis using mouse tail DNA and wild-type (forward, ATGGCATATGGAAAGTTTGTAGGT; reverse, AACATGAAACATGCCTTCTTTGTA) and mutant allele-specific primers (forward, GTTCGCAAGAACCTGATGCACA; reverse, CTAGAGCCTGTTTTGCACGTTC). Total protein extracts were prepared (Chen et al., 1998) from postnatal day 1 skeletal muscle and separated on a 3–8% NuPAGE Tris-acetate gel (Invitrogen) and subjected to Western blot analysis using polyclonal antibodies against nebulin domain M161–165 (1:50; provided by S. Labeit, Universitätsklinikum Mannheim, Mannheim, Germany) according to the manufacturer's instructions. Glyceraldehyde-3-phosphate dehydrogenase antibodies were used for normalization (1:1,000; Sigma-Aldrich).

RT-PCR analysis

Total RNA was isolated from skeletal muscle and heart tissue from 1-d-old neonatal mice by using TRIzol reagent (Invitrogen). First-strand cDNA synthesis was performed with the random primer and Superscript kit (Invitrogen). The cDNA was used as a PCR template to perform PCR by standard protocols. Specific primers for *nebulin* exons 2 and 3 (forward, TCTGTTTACAGTACTACACAGAGGA; reverse, ACAATGGTGGCGACATAATGAACAAG), 98–102 (forward, CAAAAATTGCCTATGACCTTCAGAGTGACA; reverse, TCATCCAGGGTGTAGCCATAGGCCTTGGTG), and 163 and 164 (forward, GAAGCTGCGGACCAGCGCCTTTCCAC; reverse, ACCCCGGCAGTAGACGGGTGTGATGGG) were used.

X-galactosidase staining

Fate mapping of *nebulin*-expressing cells was assessed by crossing *nebulin*$^{+/-}$ heterozygous mice with the reporter Rosa26 mouse line to generate double heterozygous *nebulin*$^{+/-}$ Rosa26 mice in which lacZ is expressed from the Rosa26 promoter after Cre-mediated recombination (Soriano, 1999). Tissue was stained for β-galactosidase activity according to the standard procedure. Tissue was fixed for 30 min at room temperature in 4% PFA in PBS and washed in PBS. Subsequently, tissue was stained overnight at 37°C using the X-galactosidase staining solution (5 mM potassium ferricyanide, 5 mM potassium ferrocyanide, 2 mM MgCl2, and 0.4% X-galactosidase in PBS) and rinsed twice in PBS. For frozen sections, tissue was frozen in optimal cutting temperature after fixation and sectioned at a thickness of 10 μm. Sections were incubated overnight at 37°C in X-galactosidase staining solution and counterstained with eosin followed by dehydration and mounting in permount. Cardiomyocytes were isolated as described previously (Kondo et al., 2006), fixed, and stained in X-galactosidase staining solution before mounting in permount. Tissue was analyzed and photographed on a dissecting microscope (SV-6; Carl Zeiss MicroImaging, Inc.) with a 35-mm camera (C-mount; Nikon).

TEM

For TEM on TA muscle, hind limbs from day 1 neonatal mice were transected midfemur and pinned to cork with the knee joint fixed at 90° and the ankle joint fixed either at 90° (neutral) or 180° (fully plantarflexed), which results in stretching of the TA muscle. After fixing overnight in 2% PFA and 2% glutaraldehyde in 0.1 M sodium cacodylate buffer, pH 7.4, the TA muscle was dissected out and cut into smaller pieces. Diaphragm muscle was dissected out and cut into smaller pieces before subsequent fixation overnight. Muscle tissue was postfixed and stained for 2 h in 1% osmium tetroxide and 1% potassium ferrocyanide followed by 1 h in 1% uranyl acetate. After dehydration in a series of ethanol and acetone, muscle tissue was embedded in Durcupan resin (EMD). Ultrathin sections (60–70 nm) were stained with lead citrate, and electron micrographs were recorded by using an electron microscope (1200EX; JEOL) operated at 80 kV.

Immunostaining

Hind limbs were fixed overnight in 4% PFA in either an unstretched or stretched position as described in the previous section. TA, EDL, gastrocnemius, and VL muscle were dissected out and incubated in 10, 15, and 30% sucrose in PBS before freezing in optimal cutting temperature. 10-μm longitudinal frozen sections were permeabilized and blocked in a solution containing 1% normal goat serum, 0.3% Triton X-100, 50 μm glycine, and 1% cold water fish gelatin (Sigma-Aldrich) in 1× PBS for 30 min followed by incubation overnight at 4°C in a humidified chamber with various antibodies in wash buffer (0.01% Triton X-100, 5 μm glycine, and 0.1% fish gelatin in PBS). Phalloidin (1:100; Sigma-Aldrich) as well as the following antibodies were used: sarcomeric α-actinin antibody EA-53 (1:1,000; Sigma-Aldrich), nebulin M161–165 (1:50; provided by S. Labeit), α-myosin F59 (1:50; Developmental Studies Hybridoma Bank), tropomodulin (polyclonal 1:50 and monoclonal E-Tmod 204; 1:100; Sung and Lin, 1994; provided by M. Sussman [San Diego State University, San Diego, CA] and A. Sung [University of California, San Diego, La Jolla, CA], respectively), tropomyosin CH1 (1:50; Sigma-Aldrich), desmin D33 (1:25; Sigma-Aldrich), and palladin (1:50; provided by C. Otey, University of North Carolina, Chapel Hill, NC). After rinsing in wash buffer, sections were incubated at room temperature for 4 h with fluorescently labeled secondary antibodies (goat anti–mouse FITC, goat anti–rabbit FITC, or goat anti–mouse RedX antibody; Sigma-Aldrich) at a final dilution of 1:100 in wash buffer. Slides were rinsed in wash buffer, dried, and mounted in Gelvatol. Confocal microscopy was performed using a confocal microscope (Radiance 2000; Bio-Rad) with a 60× plan- Apochromat NA 1.4 objective (Carl Zeiss MicroImaging, Inc.). Individual images (1,024 × 1,024) were converted to tiff format and merged as pseudocolor RGB images using Imaris (Bitplane AG).

Thin filament length analysis

Thin filament length analysis was performed by distributed deconvolution using a custom plugin written for ImageJ (National Institutes of Health [NIH]; http://rsb.info.nih.gov/ij/). This method determines the best fit of a probe-specific intensity (model) distribution to 1D myofibril fluorescence intensity profiles (line scans) by estimating the spread of light along the line scan and the positions and intensities of each probe with adjustable intensity distribution models for the entire thin filament array (I-Z-I body; Littlefield and Fowler, 2002). Image regions containing at least three stretched or hypercontracted sarcomeres were identified based on the appearance of tropomodulin doublets or phalloidin gaps (H zones). Regions were not analyzed if tropomodulin doublets or phalloidin gaps were not visible. Background-corrected line scans were calculated by averaging the intensity across the width of the myofibril for each point along the selected myofibril length by subtracting the minimum intensity above and/or below the myofibril from the mean intensity across the myofibril width. Line scans were analyzed by distributed deconvolution using model distributions for α-actinin, phalloidin, and tropomodulin as described in Littlefield and Fowler (2002). Thin filament length was defined as half the distance between tropomodulin peaks or half the width of the phalloidin bands. Based on Z-line positions in muscles costained with α-actinin and tropomodulin and corrected for possible image registration, we estimated the positional error associated with the method to ∼50 nm. For example, for gastrocnemius muscles from *nebulin*$^{-/-}$ mice, there was an estimated error of 66 nm in sarcomere lengths and of 47 nm in Z-line positions, which could not result from image misregistration.

Neonatal TA contractile testing

To provide the best estimate of muscle mechanical properties that did not reflect the progressive deterioration of the pups from days 1–11 (Fig. 3), mechanical experiments were performed on 1-d-old pups. Animals were killed by decapitation, and hind limbs were transected at the midfemur, immediately placed into a mammalian Ringer's solution (137 mM NaCl, 5 mM KCl, 24 mM $NaHCO_3$, 1 mM NaH_2PO_4, 2 mM $CaCl_2$, 1 mM $MgSO_4$, 11 mM glucose, and 10 mg/L curare), and kept on ice until tested. Pilot experiments revealed that the neonatal tendon was extraordinarily fragile and, thus, could not be secured directly to the testing apparatus. Therefore, we tested the muscle–tendon–bone unit associated with the TA muscle. Distal to the TA muscle, the tarsal bone was secured to the lever arm of a servomotor (305B; Aurora Scientific). Proximal to the TA muscle, an anodized stainless steel minutien pin (0.2-mm diameter; Fine Science Tools) was bent to a 90° angle, and the sharp end was driven down the shaft of the femur until it protruded from the femoral condyle. The blunt half was then secured with a set screw to an XYZ translator (Newport Corporation) and adjusted until both the ankle and knee joints were at 90° and the tibia was perpendicular to the foot. Once the leg was fixed in this position, the plantar flexors were severed at the Achilles tendon and dissected away. The length of the TA muscle was measured using a stereomicroscope (Leica MZ16; McBain Instruments) fitted with an eyepiece crosshair reticle, translating the chamber under the field of view from origin to insertion of the

muscle using a digital micrometer (350-712-30; Mitutoyo), and taking the mean of three measurements. Data acquisition was performed with a custom-written LabVIEW program (National Instruments) to trigger the 6-bp stimulator (Pulsar; FHC) and record force from the servomotor using a data acquisition board (PCI-6040; National Instruments) sampling at 4,000 Hz. Maximum isometric tension was measured by stimulating dorsiflexors via platinum plate electrodes with a bipolar 400-ms train of 0.3-ms pulses delivered at 100 Hz. Two measurements were taken 2 min apart and averaged. After mechanical testing, the legs were removed from the chamber, and the TA and EDL muscles were dissected and weighed. The force-time records were then analyzed by a computer algorithm written in MatLab (The MathWorks) to calculate isometric force.

Architectural measurements on neonatal TA muscle

To determine the specific force generated by each muscle, raw force was normalized by PCSA, the only anatomical value, which has been shown to be proportional to muscle force generation (Lieber and Friden, 2000). PCSA takes into account both fiber length and fiber pennation angle to yield a value that represents the total cross-sectional area of muscle fibers. This value permits comparison between the intrinsic contractile properties of muscles of different sizes. Because *nebulin*$^{-/-}$ mice are slightly smaller compared with wild-type littermates, we did not want the small size of the muscle to dominate the analysis. Thus, PCSA was calculated for each muscle using the following equation:

$$\mathrm{PCSA}\left(\mathrm{mm}^2\right) = \frac{\mathrm{M}(\mathrm{g}) \times \cos\theta}{\rho\left(\mathrm{g/mm}^3\right) \times \mathrm{L_f}\,(\mathrm{mm})}$$

where L_f is fiber length, θ is the fiber pennation angle, and ρ is muscle density. L_f was determined for each specimen using the TA L_f ratio of 0.65 (Burkholder et al., 1994). Muscle-specific tension was then calculated as muscle force/PCSA. Because normal mammalian muscle generates a specific tension of ~250 kPa, this method also allowed us to compare these neonatal muscles with their adult counterparts.

Online supplemental material

Fig. S1 shows an example of the thin filament length analysis in gastrocnemius muscle using distributed convolution. Online supplemental material is available at http://www.jcb.org/cgi/content/full/jcb.200603119/DC1.

We thank Fan Chang for technical assistance with the microscopes and Maryann Martone, Velia Fowler, Kuan Wang, Carol Gregorio, and Odile Mathieu-Costello for helpful discussions. Furthermore, we would like to thank Silvia Evans, Patrick Nahirney, Farah Sheikh, and Richard Kondo for critical reading of the manuscript.

The work was supported by NIH grants to J. Chen, R.L. Lieber, R. Littlefield, and K.U. Knowlton. TEM was carried out at the National Center for Microscopy and Imaging Research, which is supported by NIH grant RR04050.

Submitted: 3 March 2006
Accepted: 16 May 2006

References

Agbulut, O., P. Noirez, F. Beaumont, and G. Butler-Browne. 2003. Myosin heavy chain isoforms in postnatal muscle development of mice. *Biol. Cell.* 95:399–406.

Bang, M.L., R.E. Mudry, A.S. McElhinny, K. Trombitas, A.J. Geach, R. Yamasaki, H. Sorimachi, H. Granzier, C.C. Gregorio, and S. Labeit. 2001. Myopalladin, a novel 145-kilodalton sarcomeric protein with multiple roles in Z-disc and I-band protein assemblies. *J. Cell Biol.* 153:413–427.

Bang, M.L., C. Gregorio, and S. Labeit. 2002. Molecular dissection of the interaction of desmin with the C-terminal region of nebulin. *J. Struct. Biol.* 137:119–127.

Burkholder, T.J., B. Fingado, S. Baron, and R.L. Lieber. 1994. Relationship between muscle fiber types and sizes and muscle architectural properties in the mouse hind limb. *J. Morphol.* 221:177–190.

Chen, J., S.W. Kubalak, S. Minamisawa, R.L. Price, K.D. Becker, R. Hickey, J. Ross Jr., and K.R. Chien. 1998. Selective requirement of myosin light chain 2v in embryonic heart function. *J. Biol. Chem.* 273:1252–1256.

Donner, K., M. Sandbacka, V.L. Lehtokari, C. Wallgren-Pettersson, and K. Pelin. 2004. Complete genomic structure of the human nebulin gene and identification of alternatively spliced transcripts. *Eur. J. Hum. Genet.* 12:744–751.

Fock, U., and H. Hinssen. 1999. Identification and localisation of nebulin as a thin filament component of invertebrate chordate muscles. *J. Comp. Physiol. [B].* 169:555–560.

Fock, U., and H. Hinssen. 2002. Nebulin is a thin filament protein of the cardiac muscle of the agnathans. *J. Muscle Res. Cell Motil.* 23:205–213.

Fowler, V.M., C.R. KcKeown, and R.S. Fischer. 2006. Nebulin: does it measure up as a ruler? *Curr. Biol.*16: R18–R20.

Gordon, A.M., A.F. Huxley, and F.J. Julian. 1966. The variation in isometric tension with sarcomere length in vertebrate muscle fibres. *J. Physiol.* 184:170–192.

Granzier, H.L., H.A. Akster, and H.E. Ter Keurs. 1991. Effect of thin filament length on the force-sarcomere length relation of skeletal muscle. *Am. J. Physiol.* 260:C1060–C1070.

Horowits, R. 2006. Nebulin regulation of actin filament lengths: new angles. 2006. *Trends Cell Biol.* 16:121–124.

Huxley, A.F., and R.M. Simmons. 1971. Proposed mechanism of force generation in striated muscle. *Nature*. 233:533–538.

Jin, J.P., and K. Wang. 1991. Nebulin as a giant actin-binding template protein in skeletal muscle sarcomere. Interaction of actin and cloned human nebulin fragments. *FEBS Lett.* 281:93–96.

Joo, Y.M., M.A. Lee, Y.M. Lee, M.S. Kim, S.Y. Kim, E.H. Jeon, J.K. Choi, W.H. Kim, H.C. Lee, B.I. Min, et al. 2004. Identification of chicken nebulin isoforms of the 31-residue motifs and non-muscle nebulin. *Biochem. Biophys. Res. Commun.* 325:1286–1291.

Kazmierski, S.T., P.B. Antin, C.C. Witt, N. Huebner, A.S. McElhinny, S. Labeit, and C.C. Gregorio. 2003. The complete mouse nebulin gene sequence and the identification of cardiac nebulin. *J. Mol. Biol.* 328:835–846.

Kondo, R.P., D.A. Dederko, C. Teutsch, J. Chrast, D. Catalucci, K.R. Chien, and W.R. Giles. 2006. Comparison of contraction and calcium handling between right and left ventricular myocytes from adult mouse heart: a role for repolarization waveform. *J. Physiol.* 571:131–146.

Labeit, S., and B. Kolmerer. 1995. Titins: giant proteins in charge of muscle ultrastructure and elasticity. *Science*. 270:293–296.

Lieber, R.L., and J. Friden. 2000. Functional and clinical significance of skeletal muscle architecture. *Muscle Nerve*. 23:1647–1666.

Littlefield, R., and V.M. Fowler. 1998. Defining actin filament length in striated muscle: rulers and caps or dynamic stability? *Annu. Rev. Cell Dev. Biol.* 14:487–525.

Littlefield, R., and V.M. Fowler. 2002. Measurement of thin filament lengths by distributed deconvolution analysis of fluorescence images. *Biophys. J.* 82:2548–2564.

Littlefield, R., A. Almenar-Queralt, and V.M. Fowler. 2001. Actin dynamics at pointed ends regulates thin filament length in striated muscle. *Nat. Cell Biol.* 3:544–551.

Ma, K., and K. Wang. 2002. Interaction of nebulin SH3 domain with titin PEVK and myopalladin: implications for the signaling and assembly role of titin and nebulin. *FEBS Lett.* 532:273–278.

McElhinny, A.S., B. Kolmerer, V.M. Fowler, S. Labeit, and C.C. Gregorio. 2001. The N-terminal end of nebulin interacts with tropomodulin at the pointed ends of the thin filaments. *J. Biol. Chem.* 276:583–592.

McElhinny, A.S., S.T. Kazmierski, S. Labeit, and C.C. Gregorio. 2003. Nebulin: the nebulous, multifunctional giant of striated muscle. *Trends Cardiovasc. Med.* 13:195–201.

McElhinny, A.S., C. Schwach, M. Valichnac, S. Mount-Patrick, and C.C. Gregorio. 2005. Nebulin regulates the assembly and lengths of the thin filaments in striated muscle. *J. Cell Biol.* 170:947–957.

Millevoi, S., K. Trombitas, B. Kolmerer, S. Kostin, J. Schaper, K. Pelin, H. Granzier, and S. Labeit. 1998. Characterization of nebulette and nebulin and emerging concepts of their roles for vertebrate Z-discs. *J. Mol. Biol.* 282:111–123.

Moncman, C.L., and K. Wang. 1995. Nebulette: a 107 kD nebulin-like protein in cardiac muscle. *Cell Motil. Cytoskeleton*. 32:205–225.

Moncman, C.L., and K. Wang. 1996. Assembly of nebulin into the sarcomeres of avian skeletal muscle. *Cell Motil. Cytoskeleton*. 34:167–184.

Morgan, D.L., and D.G. Allen. 1999. Early events in stretch-induced muscle damage. *J. Appl. Physiol.* 87:2007–2015.

Nwe, T.M., K. Maruyama, and Y. Shimada. 1999. Relation of nebulin and connectin (titin) to dynamics of actin in nascent myofibrils of cultured skeletal muscle cells. *Exp. Cell Res.* 252:33–40.

Pfuhl, M., S.J. Winder, and A. Pastore. 1994. Nebulin, a helical actin binding protein. *EMBO J.* 13:1782–1789.

Root, D.D., and K. Wang. 1994. Calmodulin-sensitive interaction of human nebulin fragments with actin and myosin. *Biochemistry*. 33:12581–12591.

Root, D.D., and K. Wang. 2001. High-affinity actin-binding nebulin fragments influence the actoS1 complex. *Biochemistry*. 40:1171–1186.

Sam, M., S. Shah, J. Friden, D.J. Milner, Y. Capetanaki, and R.L. Lieber. 2000. Desmin knockout muscles generate lower stress and are less vulnerable to injury compared with wild-type muscles. *Am. J. Physiol. Cell Physiol.* 279:C1116–C1122.

Shimada, Y., M. Komiyama, S. Begum, and K. Maruyama. 1996. Development of connectin/titin and nebulin in striated muscles of chicken. *Adv. Biophys.* 33:223–233.

Soriano, P. 1999. Generalized lacZ expression with the ROSA26 Cre reporter strain. *Nat. Genet.* 21:70–71.

Sung, L.A., and J.J. Lin. 1994. Erythrocyte tropomodulin binds to the N-terminus of hTM5, a tropomyosin isoform encoded by the gamma-tropomyosin gene. *Biochem. Biophys. Res. Commun.* 201:627–634.

Wallgren-Pettersson, C., K. Pelin, P. Hilpela, K. Donner, B. Porfirio, C. Graziano, K.J. Swoboda, M. Fardeau, J.A. Urtizberea, F. Muntoni, et al. 1999. Clinical and genetic heterogeneity in autosomal recessive nemaline myopathy. *Neuromuscul. Disord.* 9:564–572.

Wallgren-Pettersson, C., K. Donner, C. Sewry, E. Bijlsma, M. Lammens, K. Bushby, M.L. Giovannucci Uzielli, E. Lapi, S. Odent, Z. Akcoren, et al. 2002. Mutations in the nebulin gene can cause severe congenital nemaline myopathy. *Neuromuscul. Disord.* 12:674–679.

Wang, K. 1996. Titin/connectin and nebulin: giant protein rulers of muscle structure and function. *Adv. Biophys.* 33:123–134.

Wang, K., and J. Wright. 1988. Architecture of the sarcomere matrix of skeletal muscle: immunoelectron microscopic evidence that suggests a set of parallel inextensible nebulin filaments anchored at the Z line. *J. Cell Biol.* 107:2199–2212.